Unified description of electromagnetic and α transitions in even-even nuclei

D. S. Delion[1,2,3] and A. Dumitrescu[1,4]

[1] *"Horia Hulubei" National Institute of Physics and Nuclear Engineering, 407 Atomiştilor, POB MG-6, Bucharest-Măgurele, RO-077125, România*

[2] *Academy of Romanian Scientists, 54 Splaiul Independenţei, Bucharest, RO-050094, România*

[3] *Bioterra University, 81 Gârlei str., Bucharest, RO-013724, România*

[4] *Department of Physics, University of Bucharest, 405 Atomiştilor, POB MG-11, Bucharest-Măgurele, RO-077125, România*

(Received 14 February 2013; revised manuscript received 23 March 2013; published 10 April 2013)

We describe electromagnetic and α-decay transitions to low-lying excited states in even-even nuclei within the coherent state model (CSM). We reproduced the energies and $B(E2)$ values for ground state bands in 40 daughter nuclei with known α-branching ratios to 2^+ states. To this purpose we used two parameters, namely the deformation parameter and the strength of the harmonic CSM Hamiltonian. The Hamiltonian describing the α-emission process is given by two terms. The first term describes the dynamics of the daughter nucleus. The second α-daughter component contains the monopole potential, estimated within the double folding procedure with M3Y interaction plus a repulsive core simulating Pauli principle and a quadrupole-quadrupole (QQ) interaction. The decaying states are identified with the lowest narrow outgoing resonances in this potential. The α-branching ratios to 2^+ states were reproduced by using the QQ strength depending linearly on the deformation parameter, as predicted by CSM. The theoretical intensities to 4^+ and 6^+ states are in a reasonable agreement with available experimental data. We found out that the QQ coupling strength is by one order of magnitude larger in the region above ^{208}Pb, where the α clustering is known to be stronger, in comparison to other nuclei. This formalism is able to simultaneously describe electromagnetic and α decays to excited states in spherical, transitional, and well deformed nuclei.

DOI: 10.1103/PhysRevC.87.044314 PACS number(s): 23.60.+e, 21.60.Ev, 23.20.Js, 23.20.Lv

I. INTRODUCTION

It is already a well established fact that relative values of α-decay half-lives can be satisfactorily described within the Gamow penetration picture of a preformed α particle through the Coulomb barrier [1]. In order to describe absolute half lives it is also necessary to consider the α-particle formation probability within the R-matrix theory [2–4].

For transitions between ground states the α-particle formation amplitude is a coherent superposition of many single-particle configurations, including states in continuum and therefore the decay width is not sensitive to the nuclear structure details [5,6]. The situation becomes different for transitions to excited states, because only those single-particle states that are around the Fermi surfaces are involved. Therefore decay widths to excited states are very sensitive to the structure of the wave function in the daughter nucleus. The importance of this kind of α-decay spectroscopy was recently evidenced in Ref. [7].

In order to separate the exponential dependence of the decay width upon the Q-value one extracts the barrier penetration by introducing the so-called hindrance factors (HF) [8], defined by the ratio between preformation probabilities of two nuclear states. The first attempts to estimate HFs in vibrational nuclei within the quasiparticle random-phase approximation (QRPA) were performed in Refs. [9,10]. Later on, in Ref. [11] an explanation was given for the connection between the HF of the first excited 0^+ state and the neutron number for Pb isotopes in terms of pairing vibration. More recently, a systematic analysis of α transitions to 0^+ and 2^+ states in Pb and Po isotopes was performed within the deformed density-dependent cluster model, by supposing a Boltzman distribution for the preformation factor [12]. The α-decay spectroscopy was used to investigate the 0^+ and 2^+ excited states in the Pb [13–15] and U region [16]. We analyzed some of the experimental results concerning the fine structure of 2^+ states by using the QRPA formalism in Refs. [17–19].

Let us mention that the first computations of the α-decay widths in rotational nuclei within the coupled channels approach were performed in Ref. [20]. In Ref. [21] HFs were estimated in rotational nuclei by using the Fröman approach [22] for the barrier penetration and a simple phenomenological ansatz for the preformation factor. The α-core potential was estimated by using double folding procedure in Refs. [23–25].

In several papers [26,27] we analyzed within the coupled channels formalism a more complex process, namely the double fine structure of emitted fragments in the cold fission of ^{252}Cf. The fissioning state was identified with a resonance in the interfragment potential, estimated by the double folding procedure. For the external part of the potential we used the two-body M3Y plus Coulomb interaction, while the energy was adjusted to reproduce the experimental Q value by using an internal repulsive core. We found out that the yields to excited states in both fragments are very sensitive to nuclear structure details such as the mean-field deformation and density diffusivity. Unfortunately there are only few available experimental data to be analyzed in this field [28].

On the other hand, there are many high-precision data concerning α-decay fine structure to excited states in even-even nuclei, see, e.g., [29,30]. They were analyzed within the coupled channel formalism in Refs. [31,32], by using the same double folding potential plus a repulsion simulating the Pauli principle, as for the cold fission. Later on a series

of papers were devoted to the coupled channel analysis of the α-decay fine structure [33,34], by using the double folding potential together with the Wildermuth rule to simulate the Pauli principle [35].

The aim of this paper is to give a unified description of α transitions to excited states in vibrational, transitional, and well-deformed nuclei, by using a common formalism provided by the coherent state model [36,37]. We will use the deformation parameter given by the energy level analysis to connect standard nuclear structure data to the α-decay spectroscopy.

The paper is organized according to the following plan. In Sec. II we shortly remind the main theoretical ingredients and in Sec. III we perform an analysis of energy levels, electromagnetic transitions and α-decay widths to excited states in even-even nuclei. In the last section we draw conclusions.

II. THEORETICAL BACKGROUND

In this section we summarize the main theoretical details necessary to compute energy levels and electromagnetic transition probabilities. We also give the necessary details to analize the α-decay fine structure of even-even emitters by using the coupled channels formalism.

A. Short description of the coherent state model

A coherent superposition of boson operators describing surface vibrations of a deformed nucleus was discussed in Refs. [38,39], but a complete approach describing ground, β, and γ bands was proposed in Refs. [36,37] as the coherent state model (CSM) and it was extensively developed in Refs. [40,41]. Since then it was successfully used to describe low-lying, as well as high spin states in nuclei. A recent review on this matter can be found in Ref. [42]. Here, we will shortly remind the main ingredients to describe the ground band states in even-even nuclei.

The wave function describing the intrinsic ground state is given by the following coherent superposition of quadrupole boson operators $b_{2\mu}$ with $\mu = 0$

$$|\psi_g\rangle = e^{d(b_{20}^\dagger - b_{20})}|0\rangle, \tag{2.1}$$

in terms of a deformation parameter, proportional to the static quadrupole deformation [40]

$$d = \kappa\beta_2. \tag{2.2}$$

The coherent state (2.1) can be understood as a Taylor expansion of a deformed wave function, depending on surface coordinates $\alpha_{2\mu}$, by using the boson representation of the derivative $\frac{\partial}{\partial\alpha_{2\mu}} \to \kappa(\tilde{b}_{2\mu}^\dagger - b_{2\mu})$.

Physical states, defining the ground band, can be obtained by projecting out the angular momentum

$$\varphi_J^{(g)} = \mathcal{N}_J^{(g)} P_{M0}^J \psi_g, \tag{2.3}$$

where the projection operator is defined in a standard way

$$P_{MK}^J = \sqrt{\frac{2J+1}{8\pi^2}} \int \mathrm{d}\omega D_{MK}^J(\omega)\hat{R}(\omega). \tag{2.4}$$

The key ingredient is the norm of the wave function, which can be estimated by using the following relations [41]

$$\begin{aligned} \mathcal{N}_J^{(g)} &= (2J+1)\left[I_J^{(0)}(d)\right]^{-1/2} e^{d^2/2} \\ I_J^{(0)}(d) &= \int_0^1 P_J(x) e^{d^2 P_2(x)} dx, \end{aligned} \tag{2.5}$$

where $P_J(x)$ is the Legendre polynomial. The norm can be found by a direct numerical integration, or by using a representation in terms of the degenerate hypergeometric function [41]. The expectation value of the number of bosons operator on the wave functions (2.3) is given by

$$\langle\varphi_J^{(g)}|\hat{N}|\varphi_J^{(g)}\rangle = \langle\varphi_J^{(g)}|\sum_\mu b_{2\mu}^\dagger b_{2\mu}|\varphi_J^{(g)}\rangle = d^2\mathcal{I}_J(d), \tag{2.6}$$

where we introduced the following universal function depending on deformation

$$\mathcal{I}_J(d) \equiv \frac{I_J^{(1)}(d)}{I_J^{(0)}(d)}, \quad I_J^{(1)}(d) = \frac{dI_J^{(0)}(x)}{dx}, \quad x = d^2. \tag{2.7}$$

Notice that the ground band energy spectrum

$$\begin{aligned} E_J(d) &= \langle\varphi_J^{(g)}|\hat{N}|\varphi_J^{(g)}\rangle - \langle\varphi_0^{(g)}|\hat{N}|\varphi_0^{(g)}\rangle \\ &= d^2[\mathcal{I}_J(d) - \mathcal{I}_0(d)], \end{aligned} \tag{2.8}$$

has a harmonic behavior for small values of the deformation parameter d, while at large values, $d > 3$, it has a rotational shape [41]. By using the quadrupole transition operator

$$\begin{aligned} T_{2\mu} &= q_0 Q_{2\mu} \\ Q_{2\mu} &= b_{2\mu}^\dagger + \tilde{b}_{2\mu} + a_q[(b_2^\dagger \otimes b_2^\dagger)_{2\mu} + (b_2 \otimes b_2)_{2\mu}], \end{aligned} \tag{2.9}$$

where q_0 is the charge parameter, a_q the anharmonic strength and $\tilde{b}_{2\mu} = b_{2-\mu}(-)^\mu$, the $B(E2)$ value for electromagnetic transitions connecting ground band states is given by [41]

$$\begin{aligned} &B(E2: J' \to J) \\ &= \left[\frac{1}{\hat{J}'}\langle\varphi_J^{(g)}||T_2||\varphi_{J'}^{(g)}\rangle\right]^2 \\ &= \left[q(d)\langle J'0;20|J0\rangle d\left(\frac{\hat{J}'\mathcal{N}_{J'}^{(g)}}{\hat{J}\mathcal{N}_J^{(g)}} + \frac{\hat{J}\mathcal{N}_J^{(g)}}{\hat{J}'\mathcal{N}_{J'}^{(g)}}\right)\right]^2, \end{aligned} \tag{2.10}$$

where we introduced the effective charge

$$q(d) = q_0\left(1 - \sqrt{\frac{2}{7}}a_q d\right). \tag{2.11}$$

Here $\hat{J} = \sqrt{2J+1}$ and by bracket we denoted the standard Clebsch-Gordan coefficient. The reduced matrix element is defined by the usual convention

$$\langle JM|T_{\lambda\mu}|J'M'\rangle = \frac{1}{\hat{J}}\langle J'M';\lambda\mu|JM\rangle\langle J||T_\lambda||J'\rangle. \tag{2.12}$$

B. Coupled channels approach

We generalize here the theoretical framework introduced in Ref. [31] by considering that the daughter wave function is described by CSM. Let us consider an α-decay process

$$P \rightarrow D(J) + \alpha, \tag{2.13}$$

where J denotes the spin of the excited state in the even-even axially deformed daughter nucleus. Thus, the wave function of the α-daughter system has the total spin of the initial ground state (i.e., zero)

$$\begin{aligned} \Psi(b_2, \mathbf{R}) &= \sum_J \frac{f_J(R)}{R} \mathcal{Z}_J(b_2, \Omega) \\ \mathcal{Z}_J(b_2, \Omega) &\equiv \left[\varphi_J^{(g)} \otimes Y_J(\Omega)\right]_0. \end{aligned} \tag{2.14}$$

Here, $\varphi_J^{(g)}$ is the Jth eigenstate (2.3) of the CSM Hamiltonian $H_D(b_2)$ in terms of the quadrupole boson b_2 describing the dynamics of the daughter nucleus and $\mathbf{R} \equiv (R, \Omega)$ denotes the distance between the centers of two fragments. We describe the α-daughter dynamics by using the stationary Schrödinger equation, i.e.,

$$H\Psi(b_2, \mathbf{R}) = E\Psi(b_2, \mathbf{R}). \tag{2.15}$$

The Hamiltonian describing the α-decay is written as follows

$$H = -\frac{\hbar^2}{2\mu}\nabla_R^2 + H_D(b_2) + V(b_2, \mathbf{R}), \tag{2.16}$$

where μ is the reduced mass of the dinuclear system. We estimate the interaction between nuclei as a sum of two terms

$$V(b_2, \mathbf{R}) = V_0(R) + V_2(b_2, \mathbf{R}), \tag{2.17}$$

The monopole part of the interaction is given by the same ansatz as in Ref. [31], i.e.,

$$\begin{aligned} V_0(R) &= v_a \overline{V}_0(R),\ R > R_m \\ &= c(R - R_{\min})^2 - v_0,\ R \leqslant R_m, \end{aligned} \tag{2.18}$$

where $\overline{V}_0$ is the nuclear plus Coulomb interaction, estimated by using the double folding procedure within the M3Y particle-particle interaction with Reid softcore parametrization [43–45]. Here $v_a = 1$ corresponds to a "pure" α-cluster model. By considering $v_a < 1$ one assumes an α-cluster probability less than unity, necessary to reproduce the experimental half-life. The second line is the repulsive core simulating the Pauli effect (because the α-particle can exist only on the surface) and fixing the energy of the first resonant state to the experimental Q value.

We applied the same procedure as in Ref. [31] to determine the matching radius R_m and the coordinate $R_{\min}$, corresponding to the minimal value, by using the equality between the external attractive and internal repulsion, together with their derivatives [see Eqs. (32) of this reference]. Thus, the above interaction is continuous and it depends upon only one independent parameter, due to the fact that the repulsive strength c is inverse proportional with respect to the potential depth v_0 [31].

The $\lambda = 2$ term is given by the quadrupole-quadrupole (QQ) interaction

$$\begin{aligned} V_2(b_2, \mathbf{R}) = &-C_0(R - R_{\min})\frac{dV_0(R)}{dR} \\ &\times \hat{2}[Q_2 \otimes Y_2(\Omega)]_0. \end{aligned} \tag{2.19}$$

By using the orthonormality of angular functions entering the superposition (2.14) one obtains in a standard way the coupled system of differential equations for radial components [46]

$$\frac{d^2 f_J(R)}{d\rho_J^2} = \sum_{J'} A_{JJ'}(R) f_{J'}(R), \tag{2.20}$$

where the coupling matrix is given by

$$\begin{aligned} A_{JJ'}(R) = &\left[\frac{J(J+1)}{\rho_J^2} + \frac{V_0(R)}{E - E_J} - 1\right]\delta_{JJ'} \\ &+ \frac{1}{E - E_J}\langle \mathcal{Z}_J | V_2(b_2, \mathbf{R}) | \mathcal{Z}_{J'} \rangle, \end{aligned} \tag{2.21}$$

in terms of the reduced radius

$$\rho_J = \kappa_J R, \kappa_J = \sqrt{\frac{2\mu(E - E_J)}{\hbar^2}}. \tag{2.22}$$

The matrix element of the particle-core coupling entering Eq. (2.21) was derived in Ref. [36] and it is proportional to the reduced matrix element defining electromagnetic transition (2.10), but with a different anharmonic parameter

$$\begin{aligned} \langle \mathcal{Z}_J | V_2(b_2, \mathbf{R} | \mathcal{Z}_{J'} \rangle &= -C_0(R - R_{\min})\frac{dV_0(R)}{dR}\frac{1}{\hat{2}\hat{J}\hat{J}'} \\ &\times \left\langle \varphi_J^{(g)} \middle|| Q_2 \middle|| \varphi_{J'}^{(g)} \right\rangle \langle Y_J || Y_2 || Y_{J'} \rangle \\ &= -C(d)(R - R_{\min})\frac{dV_0(R)}{dR}\frac{d}{\sqrt{4\pi}}\frac{\hat{J}}{\hat{J}'} \\ &\times \langle J0; 20 | J'0 \rangle^2 \left(\frac{\hat{J}'\mathcal{N}_{J'}^{(g)}}{\hat{J}\mathcal{N}_J^{(g)}} + \frac{\hat{J}\mathcal{N}_J^{(g)}}{\hat{J}'\mathcal{N}_{J'}^{(g)}}\right), \end{aligned} \tag{2.23}$$

where we defined the effective α-daughter coupling strength

$$C(d) = C_0\left(1 - \sqrt{\frac{2}{7}}a_\alpha d\right). \tag{2.24}$$

C. Decay widths

All measured decay widths are by many orders of magnitude smaller than the corresponding Q values. Therefore the stationarity is a very good approach and an α-decaying state can be identified with a narrow resonant solution of the system (2.20), containing only outgoing components. Let us first define the internal and external fundamental solutions satisfying the following boundary conditions, respectively

$$\begin{aligned} \mathcal{R}_{JI}(R) &\overset{R \rightarrow R_0}{\longrightarrow} \delta_{JI}\varepsilon_J, \\ \mathcal{H}_{JI}^{(+)}(R) &\equiv \mathcal{G}_{JI}(R) + i\mathcal{F}_{JI}(R) \overset{R \rightarrow \infty}{\longrightarrow} \delta_{JI}H_J^{(+)}(\kappa_J R) \\ &\equiv \delta_{JI}\left[G_J(\kappa_J R) + iF_J(\kappa_J R)\right]. \end{aligned} \tag{2.25}$$

Here, R_0 is a radius inside the internal repulsive potential and ε_J are arbitrary small numbers. The index J labels the component and I solution, $G_J(\kappa_J R)$, $F_J(\kappa_J R)$ are the irregular and regular spherical Coulomb wave functions, respectively, depending on the momentum κ_J in the channel J.

Each component of the solution is built as a superposition of N independent fundamental solutions. We impose the matching conditions at some radius R_1 inside the barrier

$$\begin{aligned} f_J(R_1) &= \sum_I \mathcal{R}_{JI}(R_1) M_I = \sum_I \mathcal{H}^{(+)}_{JI}(R_1) N_I \\ \frac{df_J(R_1)}{dR} &= \sum_I \frac{d\mathcal{R}_{JI}(R_1)}{dR} M_I = \sum_I \frac{d\mathcal{H}^{(+)}_{JI}(R_1)}{dR} N_I, \end{aligned} \tag{2.26}$$

where N_I are called scattering amplitudes. The conditions (2.26) give the following secular equation

$$\begin{vmatrix} \mathcal{R}(R_1) & \mathcal{H}^{(+)}(R_1) \\ \frac{d\mathcal{R}(R_1)}{dR} & \frac{d\mathcal{H}^{(+)}(R_1)}{dR} \end{vmatrix} \approx \begin{vmatrix} \mathcal{R}(R_1) & \mathcal{G}(R_1) \\ \frac{d\mathcal{R}(R_1)}{dR} & \frac{d\mathcal{G}(R_1)}{dR} \end{vmatrix} = 0. \tag{2.27}$$

The first condition is fulfilled for complex energies, determining the resonant states. They practically coincide with the real scattering resonant states, due to the fact that the imaginary parts of energies are much smaller than the corresponding real parts, corresponding to vanishing regular Coulomb functions F_J inside the barrier. The roots of the equation (2.27) do not depend upon the matching radius R_1, because both internal and external solutions satisfy the same Schrödinger equation. The unknown coefficients M_I, N_I are determined from the normalization of the wave function in the internal region

$$\sum_J \int_{R_0}^{R_2} |f_J(R)|^2 dR = 1, \tag{2.28}$$

where R_2 is the external turning point. All known half-lives in α emission are much larger that the characteristic nuclear time $T_{\min} \approx 10^{-6}\text{s} \gg T_N \approx 10^{-22}\text{s}$. Thus, any α-decaying state practically behaves like a bound state, having an exponential decrease versus radius inside the barrier.

From the continuity equation one obtains the total decay width as a sum of partial widths

$$\begin{aligned} \Gamma &= \sum_J \Gamma_J = \sum_J \hbar v_J \lim_{R\to\infty} |f_J(R)|^2 \\ &= \sum_J \hbar v_J |N_J|^2, \end{aligned} \tag{2.29}$$

where v_J is the center of mass velocity at infinity in the channel J, i.e.,

$$v_J = \frac{\hbar \kappa_J}{\mu}. \tag{2.30}$$

III. NUMERICAL APPLICATION

We will analyze the α-decay widths to ground band states in even-even nuclei. To this purpose we should first determine the deformation parameter d. We use the simplest ansatz of the CSM Hamiltonian, given by the harmonic term [42]

$$H_D(b_2) = A_1 \hat{N} = A_1 \sum_\mu b^\dagger_{2\mu} b_{2\mu}, \tag{3.1}$$

depending upon the strength parameter A_1 and the deformation d. Notice that in Ref. [42] it was used a second strength parameter multiplying angular momentum squared. This ansatz gives slightly better results especially for small deformations, but our analysis has shown that the systematics concerning A_1 and the α-daughter interaction strengths becomes more scattered. Moreover, one parameter description of the CSM Hamiltonian allows us to derive an universal relation for the energy ratio

$$\frac{E_{J+2}}{E_J} = \frac{\mathcal{I}_{J+2}(d) - \mathcal{I}_0(d)}{\mathcal{I}_J(d) - \mathcal{I}_0(d)}, \tag{3.2}$$

in terms of the function (2.7), depending only on the deformation parameter d.

We determined the optimal values of these parameters for each nucleus by using the fitting procedure for the energies of $J = 2^+, 4^+, 6^+, 8^+$ ground band states. In our calculations we used the nuclei given in Table I, where we selected all emitters with known experimental values for α-transitions to the first excited 2^+ state. In the sixth column of the Table I we give the results for the CSM deformation parameter d and in the seventh column the strength parameter A_1. These values are close to the results of Ref. [42]. In Fig. 1(a) we plotted the deformation parameter d as a function of the standard quadrupole deformation parameter β_2 of Ref. [47]. This dependence can be fitted by two straight lines, corresponding to $N > 126$ (filled circles) and $N < 126$ (open circles), thus proving that the relation (2.2) is valid for given regions. It is interesting to point out on the fact that the deformation parameter d is strongly correlated to the Casten parameter $P = N_p N_n/(N_p + N_n)$ [48], where N_τ is the number of valence nucleons above the closest spherical shell. This behavior can be seen in Fig. 1(b).

In Ref. [7] it is shown that a parameter of the variable moment of inertia (VMI) model [49] that is related to the stiffness (rigidity) of the nucleus, is well correlated with the parameter P of Casten. Within the VMI model, the energy of the yrast states is described as a function of the angular velocity

$$E = \tfrac{1}{2}\omega^2\left(J_0 + \tfrac{3}{2}\omega^2 J_1\right). \tag{3.3}$$

Here, J_0 is almost equal to the moment of inertia derived from the energy of the 2^+_1 state state, while the inverse of J_1 is twice the value of a stiffness parameter measuring the rigidity of the nucleus. In Fig. 2 we plotted the quantity $1000/J_1$ (rigidity parameter) as a function of the deformation parameter d for the region $N > 126$. Here, one clearly sees two regions of linear correlation, corresponding to small and large deformations, separated by $d = 2$. An interesting feature is that the rigidity parameter increases not only at large, but also at small deformations.

It turns out that the strength parameter A_1 is not independent from d. Their dependence has a parabolic correlation for $N > 126$ (filled circles), as can be seen from Fig. 3.

TABLE I. Deformation parameters β_2 and d, the parameter of the CSM Hamiltonian A_1, the α-core coupling parameter C, experimental and predicted intensities of α transitions I_J to $J = 2^+, 4^+, 6^+$ states.

n	Z	N	A	β_2	d	A_1 (keV)	C	$I_{2^+}^{\exp}$	$I_{4^+}^{\exp}$	$I_{4^+}^{\text{pred}}$	$I_{6^+}^{\exp}$	$I_{6^+}^{\text{pred}}$
1	76	96	172	0.190	2.085	572.757	0.043	2.585	-	8.844	-	7.616
2	76	98	174	0.226	2.262	492.509	0.131	1.270	-	4.863	-	8.679
3	78	98	176	0.171	1.803	408.928	0.027	3.268	-	6.450	-	5.443
4	78	100	178	0.254	2.290	502.074	0.044	2.138	-	6.211	-	7.295
5	78	102	180	0.265	2.435	556.229	0.028	2.394	-	5.567	-	5.015
6	84	112	196	0.136	1.551	537.982	0.027	4.222	-	8.851	-	8.063
7	84	114	198	0.122	0.930	565.044	0.116	4.000	-	9.419	-	14.120
8	84	132	216	0.020	0.877	414.220	0.359	2.959	-	6.698	-	11.166
9	84	134	218	0.039	0.900	441.822	0.511	3.108	-	7.170	-	12.191
10	86	130	216	0.008	0.906	405.170	0.371	1.996	-	4.974	-	9.300
11	86	132	218	0.040	1.532	385.309	0.377	1.510	-	4.389	-	8.449
12	86	134	220	0.111	1.835	398.646	0.410	1.270	-	4.146	-	8.374
13	86	136	222	0.137	2.047	410.960	0.397	1.233	-	4.335	-	9.001
14	88	130	218	0.020	1.388	405.293	0.338	1.510	-	4.231	-	8.043
15	88	132	220	0.103	1.959	344.753	0.406	0.619	-	2.678	-	5.806
16	88	134	222	0.130	2.353	376.272	0.258	0.519	-	2.725	-	6.194
17	88	136	224	0.164	2.616	402.858	0.280	0.426	-	2.607	-	6.132
18	90	132	222	0.111	2.018	391.376	0.256	0.753	-	3.141	-	6.664
19	90	134	224	0.164	2.519	416.728	0.275	0.383	-	2.426	-	5.751
20	90	136	226	0.173	2.895	464.030	0.237	0.324	2.249	2.339	5.984	6.069
21	90	138	228	0.182	3.068	448.686	0.192	0.334	2.356	2.419	6.126	5.606
22	90	140	230	0.198	3.499	555.671	0.148	0.400	2.553	2.623	-	6.301
23	90	142	232	0.207	3.608	555.049	0.123	0.455	2.453	2.786	-	6.190
24	90	144	234	0.215	3.767	615.270	0.095	0.577	3.006	3.162	-	6.091
25	92	138	230	0.199	3.508	543.762	0.126	0.327	2.230	2.350	-	5.187
26	92	140	232	0.207	3.727	576.660	0.109	0.355	2.585	2.465	4.539	5.037
27	92	142	234	0.215	3.787	547.554	0.096	0.389	2.830	2.489	4.374	5.314
28	92	144	236	0.215	3.987	640.331	0.090	0.429	2.932	2.680	4.829	5.086
29	92	146	238	0.215	3.990	636.205	0.073	0.539	2.898	2.959	4.775	6.100
30	94	142	236	0.215	4.012	640.608	0.082	0.390	3.135	2.452	3.705	4.529
31	94	144	238	0.215	4.248	718.871	0.065	0.471	3.325	2.740	4.378	4.560
32	94	146	240	0.223	4.138	659.043	0.087	0.510	3.541	2.735	4.339	4.095
33	94	148	242	0.224	4.196	706.800	0.050	0.664	3.313	3.267	-	4.658
34	94	150	244	0.224	3.864	614.529	0.059	0.657	3.032	3.205	-	5.045
35	96	146	242	0.224	4.500	770.881	0.046	0.585	2.723	2.999	3.695	3.663
36	96	148	244	0.234	4.331	731.418	0.044	0.653	2.309	3.037	-	3.869
37	96	150	246	0.234	4.397	752.888	0.038	0.748	2.450	3.238	3.927	3.806
38	96	152	248	0.235	4.260	710.991	0.040	0.729	2.545	3.249	4.624	4.534
39	98	150	248	0.235	3.889	558.267	0.040	0.748	1.938	3.296	3.563	4.381
40	98	152	250	0.245	4.184	678.191	0.035	0.777	2.016	3.406	4.110	3.912

Concerning the other region with $N < 126$ (open circlers) the data are clustered around a common value $A_1 \approx 0.55$ MeV.

In order to check the quality of this approach we plotted the relation (3.2) by solid lines for $J = 2$ in Fig. 4(a) and $J = 4$ in Fig. 4(b). It is nicely fulfilled by all experimental data, with a higher accuracy for $N > 126$ (filled circles) than for $N < 126$ (open circles). This proves the predicting power of the CSM concerning the energies of the ground band from vibrational to well-deformed nuclei. In Ref. [42] the analysis was extended to β and γ bands, but unfortunately the amount of α-decay data is very limited for them.

We used the values of the deformation parameter d to estimate the effective charge by using the values $B(E2 : 2 \to 0)$ given by Eq. (2.10). The values are given in Fig. 5 by filled circles for for $N > 126$ and by open circles for $N < 126$. They follow the linear dependence predicted by Eq. (2.11), given by the solid lines

$$\begin{aligned} q(d) &= 0.261d + 3.651, \quad \sigma = 0.249, \quad N > 126 \\ &\quad 0.281d + 5.214, \quad \sigma = 0.332, \quad N < 126. \end{aligned} \tag{3.4}$$

The slope of the linear dependence determines the anharmonicity parameter a_q. One sees that it has relative small values, i.e.,

$$\begin{aligned} a_q &= -0.134, \quad N > 126 \\ &= -0.101, \quad N < 126. \end{aligned} \tag{3.5}$$

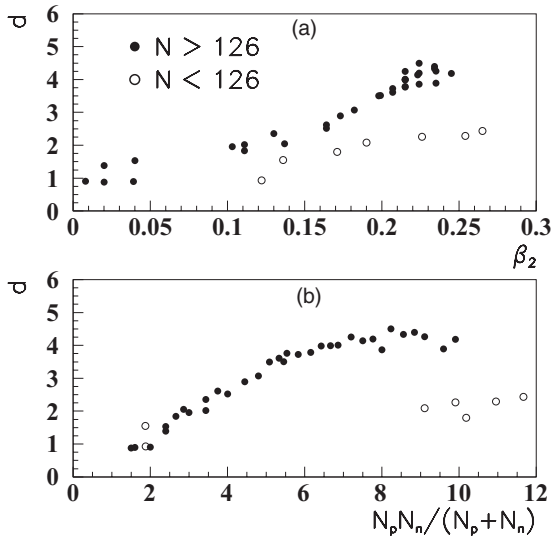

FIG. 1. (a) Deformation parameter d versus the quadrupole deformation β_2 [47]. (b) Deformation parameter d versus Casten parameter $P = N_p N_n/(N_p + N_n)$.

The main purpose of this paper is to use the CSM deformation parameter d, in order to determine the α-decay fine structure, defined by the logarithm of the ratio between decay widths to ground and J^+ states, respectively

$$I_J \equiv \log_{10} \frac{\Gamma_0}{\Gamma_J}, \tag{3.6}$$

where partial widths are given by Eq. (2.29). We call this quantity the intensity of the α decay to the Jth state. We considered the value $v_a = 1$ multiplying the monopole interaction (2.18), corresponding to a preformed cluster, because the above ratio (3.6) practically does not depend on this value, as it was shown in Ref. [31]. In the same reference it was also evidenced a strong correlation between c and v_0 in Eq. (2.19). Thus, in our calculations we fixed the value of the repulsive strength $c = 50$ MeV, as in Ref. [32], and changed the only remaining free parameter v_0 in order to reproduce the Q value for each α decay.

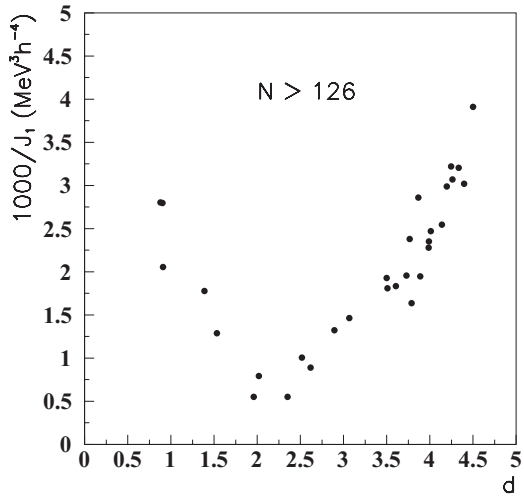

FIG. 2. Rigidity parameter $1000/J_1$, where J_1 is defined by Eq. (3.3), versus the deformation parameter d for the region $N > 126$.

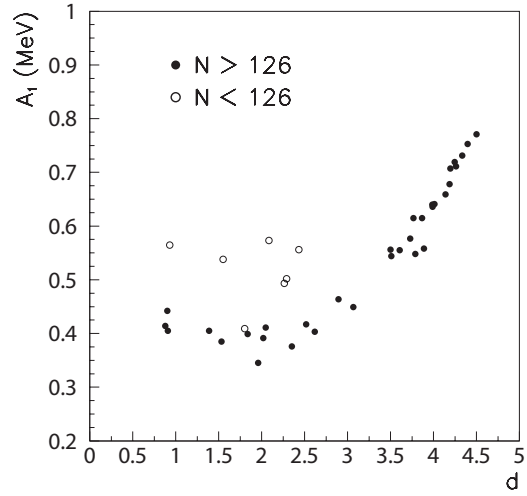

FIG. 3. Hamiltonian parameter A_1 versus the deformation parameter d.

By changing the effective α-daughter coupling strength $C(d)$, we reproduced the available experimental quadrupole intensities I_2, given by the eighth column of the Table I. In Fig. 6(a) we plotted the values of this strength as a function of the deformation d. They can be fitted by two linear dependencies

$$\begin{aligned} C &= -0.121d + 0.566, \quad N > 126 \\ &= -0.026d + 0.110, \quad N < 126, \end{aligned} \tag{3.7}$$

with an error $\sigma = 0.040$. Thus, we indeed obtained the linear dependence of the α-daughter QQ coupling strength with a negative slope, predicted by Eq. (2.24). Notice that for the region $N < 126$ the values belong a narrow interval of small

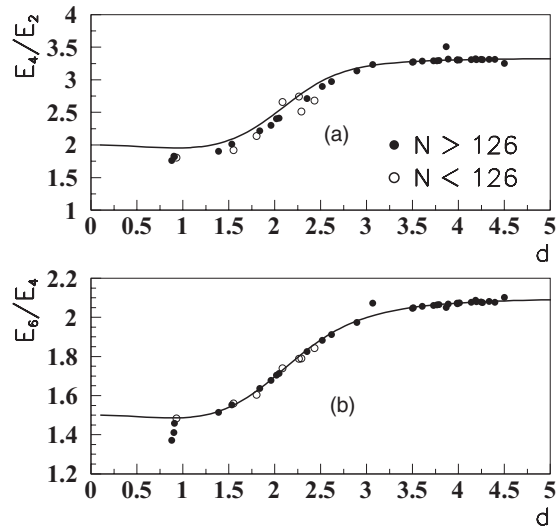

FIG. 4. (a) Theoretical ratio E_4/E_2 versus the deformation parameter d (solid line). By filled circles are given experimental values for the region $N > 126$ and by open circles for $N < 126$. (b) Same as in (a) but for the ratio E_6/E_4.

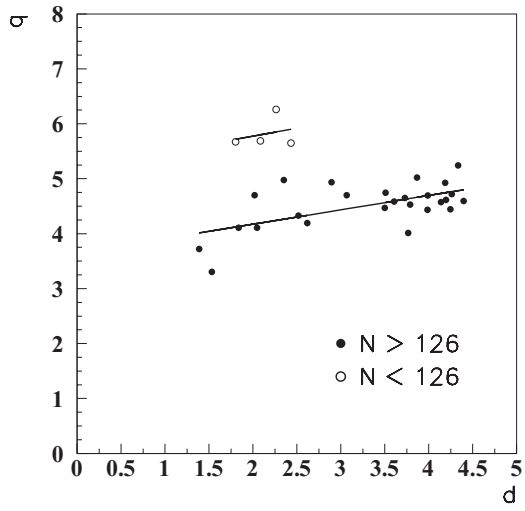

FIG. 5. Effective charge (2.11) versus the deformation parameter d. By filled circles are plotted the values for $N > 126$ and by open circles for $N < 126$. By solid lines are given the corresponding linear fits.

values $C \in [0.05, 0.1]$. As in the case of energy levels, the error diminishes for larger deformations. This dependence proves the fact that in α decay the anharmonic effects are much stronger with respect to electromagnetic transitions and similar for the two regions, i.e.,

$$\begin{aligned} a_\alpha &= 0.402, \quad N > 126 \\ &= 0.448, \quad N < 126. \end{aligned} \tag{3.8}$$

It turns out that the QQ strength can also be related to the mass number A. In Fig. 6(b) we give the dependence of this strength versus A. It can be nicely approximated by two dependencies as follows

$$\begin{aligned} C &= 0.00040(A-248)^2 + 0.033, \quad N > 126 \\ &= 0.00063(A-170) + 0.052, \quad N < 126, \end{aligned} \tag{3.9}$$

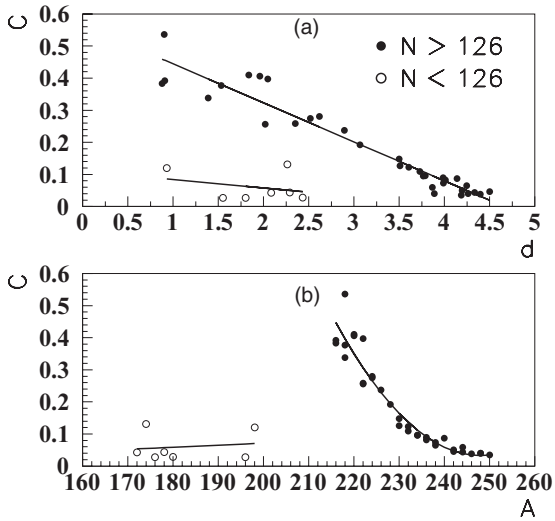

FIG. 6. (a) α-daughter QQ coupling strength C defined by Eq. (2.24) versus the deformation parameter d. (b) Same as in (a), but for the mass number A.

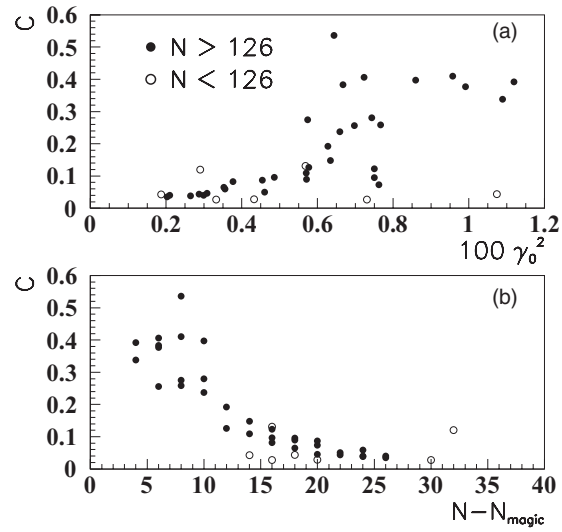

FIG. 7. (a) α-daughter QQ coupling strength C defined by Eq. (2.24) versus the α-particle probability (3.10). (b) Same as in (a), but versus $N - N_{\rm magic}$, where $N_{\rm magic} = 126$ for $N > 126$, $N_{\rm magic} = 82$ for $N < 126$.

with the same error $\sigma = 0.040$. The α-daughter QQ coupling is stronger for nuclei above ^{208}Pb, where $C \approx 0.5$, i.e., in the region where the α clustering is larger [50]. It decreases by one order of magnitude around the mass region $A = 240$. By crossing the shell closure to the region $N < 126$ one notices a jump of one order of magnitude, up to the value $C \approx 0.05$. Let us mention that for $N > 126$ this behavior is similar to the dependence of the reduced width squared (called α-particle probability) for transitions connecting ground states with $J = 0$, defined as follows

$$\gamma_J^2 = \frac{\Gamma_J}{2P_J}, \tag{3.10}$$

where P_J is the Coulomb penetrability computed at the touching radius [50]. Indeed, it turns out that the α-daughter coupling strength is proportional to the α-particle probability, but with different slopes for $N > 126$ (dark circles) and $N < 126$ (open symbols), as it can be seen from Fig. 7(a). In spite of this different behavior, the dependence versus the number of neutrons above the closed shell $N_{\rm magic}$ is common for both regions, as can be seen in Fig. 7(b).

We used these values of the α-daughter strength $C(d)$ reproducing I_2 values in order to predict the intensities I_4 and I_6. They are given in Table I and plotted in Fig. 8 by dark symbols versus the index n. These values reproduce the available experimental data, plotted by open circles, with a reasonable accuracy. This proves that this relatively simple model is able to simultaneously describe all available experimental α-decay intensities to excited states within a range of four orders of magnitude.

In order to extract the influence of the Coulomb barrier one defines the logarithm of the hindrance factors (HF) as follows

$$\log_{10} HF_J \equiv \log_{10} \frac{\gamma_0^2}{\gamma_J^2} = \log_{10} I_J - \log_{10} \frac{P_0}{P_J}, \tag{3.11}$$

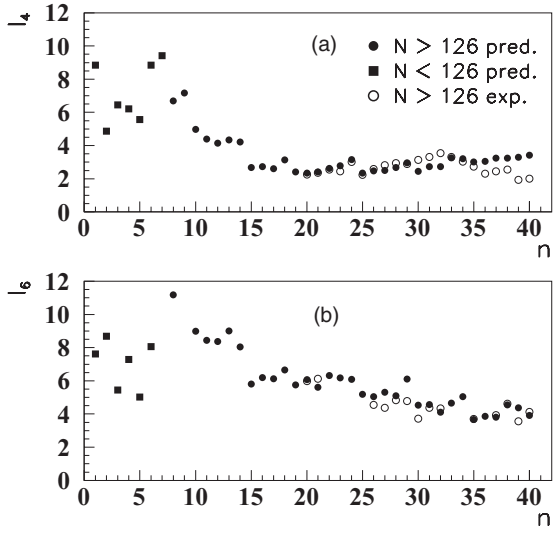

FIG. 8. (a) Predicted intensity I_4, by using the coupling strength $C(d)$ reproducing the corresponding value I_2, versus the index n in the first column of Table I. (b) Same as in (a), but for I_6.

where we used the standard representation (3.10). In Fig. 9 we plotted $\log_{10} HF_J$ versus the index n for $J = 2$ (a) and $J = 4$ (b). One notices the close resemblance with the values I_J given in Fig. 8. They are shifted by a factor given by the penetrability ratio in Eq. (3.11).

Let us analyze more carefully the region $n = 35$–40, where the predicted I_4 intensities overestimate the experimental values. In Fig. 10(a) we plotted experimental I_4 values versus the deformation parameter d. We used filled symbols for $n = 25$–29 ($Z = 92$), $n = 30$–34 ($Z = 94$) and open symbols for $n = 35$–38 ($Z = 96$), $n = 39$–40 ($Z = 98$). One clearly sees two regions corresponding to filled and open symbols, respectively. They are described by two parallel regression lines. This fact is confirmed by a similar plot in Fig. 10(b), but versus the rigidity parameter $1000/J_1$, which is proportional to d, as seen in Fig. 2. The I_2 intensities have a different pattern.

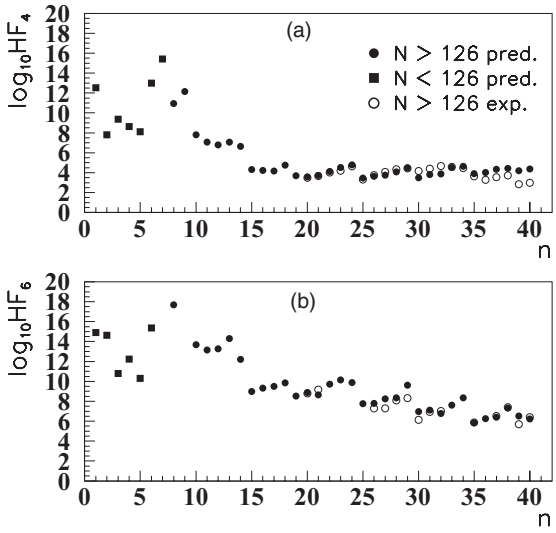

FIG. 9. Same as in Fig. 8, but for $\log_{10} HF_J$ defined by Eq. (3.11).

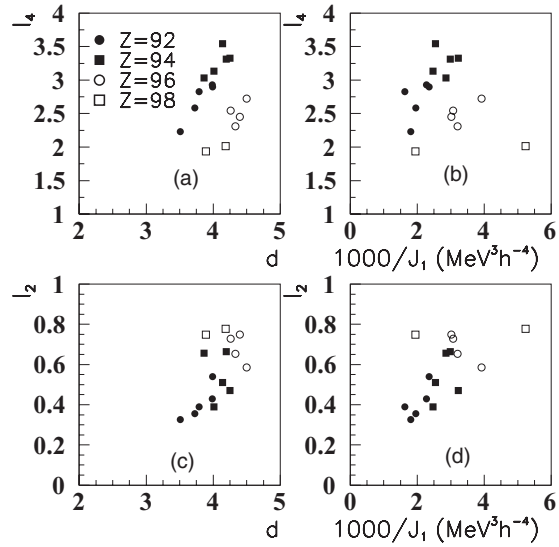

FIG. 10. (a) Experimental intensity I_4 as a function of the deformation parameter d for $Z = 92$, 94 (filled symbols) and $Z = 96$, 98 (open symbols). (b) Same as in (a), but versus the the rigidity parameter $1000/J_1$, where J_1 is defined by Eq. (3.3). (c) Same as in (a), but for I_2. (d) Same as in (b), but for I_2.

The two regions still remain separated for the corresponding I_2 values, as can be seen in Fig. 10(c) for the dependence versus d, but the data belong to the same regression line. This qualitative difference between I_2 and I_4 intensities as functions of the deformation parameter d explains why the I_4 values cannot be fully predicted by using I_2 values with a common parametrization. Anyway, this is a nice confirmation of the connection between electromagnetic and α-transition properties induced by the deformation parameter.

IV. CONCLUSION

We analyzed in this paper the available experimental α-decay widths to excited states by using the CSM formalism. In this way we described in an unified way vibrational, transitional, and well-deformed nuclei. We considered all nuclei (40) where α-decay width to the first 2^+ state is experimentally known. We have shown that the simplest harmonic CSM Hamiltonian is able to describe all available energy level ratios in terms of the deformation parameter d, proportional to the standard quadrupole parameter β_2. We also evidenced the proportionality between the CSM deformation and VMI rigidity parameters. We then described the α-decay fine structure within the coupled channel formalism by using monopole plus quadrupole terms. The attractive part was described within the double folding procedure with M3Y interaction. The Pauli principle was simulated by a repulsive potential depending on one independent parameter. The first narrow resonant state in the resulting pocketlike potential was identified with an α-decaying state. Its eigenvalue was fixed to the experimental Q value, by using the depth of the monopole repulsive potential.

It turns out that the reduced matrix describing $B(E2)$ values enters the structure of the matrix coupling the α-decay

channels. We reproduced the α intensity to the 2^+ state by using the QQ strength parameter. Its linear dependence on the deformation parameter confirms the CSM prediction. The QQ interaction strength has a jump of one order of magnitude by crossing the magic neutron number $N = 126$. In the region above to ^{208}Pb, i.e., for nuclei with largest α-clustering components, it has the strongest value and diminishes again by one order of magnitude for $A = 240$. By using these values we were able to reproduce experimental intensities to 4^+ and 6^+ states with a reasonable accuracy and we made theoretical predictions for the other α emitters. A comparison between I_4 and I_2 intensities revealed their different behavior versus the deformation parameter d.

ACKNOWLEDGMENTS

This work was supported by a grant of the Romanian Ministry of Education and Research, CNCS UEFISCDI, Project No. PN-II-ID-PCE-2011-3-0092. Discussions with Professor A. A. Raduta and Professor D. Bucurescu (Bucharest) are gratefully acknowledged.

[1] G. Gamow, Z. Phys. **51**, 204 (1928).
[2] A. M. Lane and R. G. Thomas, Rev. Mod. Phys. **30**, 257 (1958).
[3] H. J. Mang, Phys. Rev. **119**, 1069 (1960).
[4] A. Sandulescu, Nucl. Phys. A **37**, 332 (1962).
[5] J. K. Poggenburg, H. J. Mang, and J. O. Rasmussen, Phys. Rev. **181**, 1697 (1969).
[6] D. S. Delion, A. Săndulescu, and W. Greiner, Phys. Rev. C **69**, 044318 (2004).
[7] D. Bucurescu and N. V. Zamfir, Phys. Rev. C **86**, 067306 (2012).
[8] J. O. Rasmussen, Phys. Rev. **113**, 1593 (1959).
[9] A. Săndulescu and O. Dumitrescu, Phys. Lett. **19**, 404 (1965); Phys. Lett. B **24**, 212 (1967).
[10] M. I. Cristu, O. Dumitrescu, N. I. Pyatov, and A. Săndulescu, Nucl. Phys. A **130**, 31 (1969).
[11] D. S. Delion, A. Florescu, M. Huyse, J. Wauters, P. Van Duppen (ISOLDE Collaboration), A. Insolia, and R. J. Liotta, Phys. Rev. Lett. **74**, 3939 (1995); Phys. Rev. C **54**, 1169 (1996).
[12] C. Xu and Z. Z. Ren, Phys. Rev. C **75**, 044301 (2007).
[13] J. Wauters, P. Dendooven, P. Decrock, M. Huyse, R. Kirchner, O. Klepper, G. Reusen, E. Roeckl, and P. Van Duppen, Z. Phys. A **342**, 277 (1992); J. Wauters, P. Dendooven, M. Huyse, G. Reusen, P. Lievens, and P. Van Duppen (ISOLDE Collaboration), *ibid.* **344**, 29 (1992); J. Wauters, P. Dendooven, M. Huyse, G. Reusen, P. Van Duppen, R. Kirchner, O. Klepper, and E. Roeckl, *ibid.* **345**, 21 (1993); J. Wauters, P. Dendooven, M. Huyse, G. Reusen, P. Van Duppen, and P. Lievens, Phys. Rev. C **47**, 1447 (1993); J. Wauters, N. Bijnens, H. Folger, M. Huyse, H. Y. Hwang, R. Kirchner, J. von Schwarzenberg, and P. Van Duppen, *ibid.* **50**, 2768 (1994); J. Wauters, N. Bijnens, P. Dendooven, M. Huyse, H. Y. Hwang, G. Reusen, J. von Schwarzenberg, P. Van Duppen, R. Kirchner, and E. Roeckl, Phys. Rev. Lett. **72**, 1329 (1994).
[14] N. Bijnens *et al.*, Phys. Rev. Lett. **75**, 4571 (1995).
[15] R. G. Allatt *et al.*, Phys. Lett. B **437**, 29 (1998).
[16] C. F. Liang, R. K. Sheline, P. Paris, M. Hussonnois, J. F. Ledu, and D. B. Isabelle, Phys. Rev. C **49**, 2230 (1994).
[17] D. S. Delion and R. J. Liotta, Phys. Rev. C **56**, 1782 (1997).
[18] D. S. Delion and J. Suhonen, Phys. Rev. C **64**, 064302 (2001).
[19] S. Peltonen, D. S. Delion, and J. Suhonen, Phys. Rev. C **71**, 044315 (2005).
[20] J. O. Rasmussen and B. Segal, Phys. Rev. **103**, 1298 (1956).
[21] H. M. A. Radi, A. A. Shihab-Eldin, J. O. Rasmussen, and Luiz F. Oliveira, Phys. Rev. Lett. **41**, 1444 (1978).
[22] P. O. Fröman, Mat. Fys. Skr. Dan. Vid. Selsk. **1**, No. 3 (1957).
[23] R. Neu and F. Hoyler, Phys. Rev. C **46**, 208 (1992).
[24] H. Abele and G. Staudt, Phys. Rev. C **47**, 742 (1993).
[25] Dao T. Khoa, Phys. Rev. C **63**, 034007 (2001).
[26] D. S. Delion, A. Săndulescu, S. Mişicu, F. Cârstoiu, and W. Greiner, Phys. Rev. C **64**, 041303(R) (2001); J. Phys. G **28**, 289 (2002).
[27] D. S. Delion, A. Săndulescu, and W. Greiner, Phys. Rev. C **68**, 041303(R) (2003).
[28] A. Săndulescu, A. Florescu, F. Cârstoiu, W. Greiner, J. H. Hamilton, A. V. Ramayya, and B. R. S. Babu, Phys. Rev. C **54**, 258 (1996).
[29] Y. A. Akovali, Nucl. Data Sheets **84**, 1 (1998).
[30] V. Yu. Denisov and A. A. Khudenko, At. Data Nucl. Data Tables **95**, 815 (2009).
[31] D. S. Delion, S. Peltonen, and J. Suhonen, Phys. Rev. C **73**, 014315 (2006).
[32] S. Peltonen, D. S. Delion, and J. Suhonen, Phys. Rev. C **78**, 034608 (2008).
[33] D. D. Ni and Z. Z. Ren, Phys. Rev. C **80**, 051303(R) (2009); **81**, 064318 (2010); **83**, 067302 (2011).
[34] X. Zhang, C. Xu, and Z. Z. Ren, Phys. Rev. C **84**, 044312 (2011).
[35] C. Xu and Z. Z. Ren, Phys. Rev. C **73**, 041301(R) (2006); Nucl. Phys. A **778**, 1 (2006).
[36] A. A. Raduta and R. M. Dreizler, Nucl. Phys. A **258**, 109 (1976).
[37] A. A. Raduta, V. Ceausescu, and R. M. Dreizler, Nucl. Phys. A **272**, 11 (1976).
[38] P. O. Lipas and J. Savolainen, Nucl. Phys. A **130**, 77 (1969).
[39] P. O. Lipas, P. Haapakoski, and T. Honkaranta, Phys. Scr. **13**, 339 (1976).
[40] A. A. Raduta, V. Ceausescu, A. Gheorghe, and R. M. Dreizler, Phys. Lett. B **99**, 444 (1981).
[41] A. A. Raduta, V. Ceausescu, A. Gheorghe, and R. M. Dreizler, Nucl. Phys. A **381**, 253 (1982).
[42] A. A. Raduta, R. Budaca, and Amand Faessler, Ann. Phys. (NY) **327**, 671 (2012).
[43] G. Bertsch, J. Borysowicz, H. McManus, and W. G. Love, Nucl. Phys. A **284**, 399 (1977).
[44] G. R. Satchler and W. G. Love, Phys. Rep. **55**, 183 (1979).
[45] F. Cârstoiu and R. J. Lombard, Ann. Phys. (NY) **217**, 279 (1992).
[46] D. S. Delion, *Theory of particle and cluster emission* (Springer-Verlag, Berlin, 2010).
[47] P. Moller and J. R. Nix, Nucl. Phys. A **272**, 502 (1995).
[48] R. F. Casten, D. S. Brenner, and P. E. Haustein, Phys. Rev. Lett. **58**, 658 (1987).
[49] M. A. J. Mariscotti, G. Scharff-Goldhaber, and B. Buck, Phys. Rev. **178**, 1864 (1969); G. Scharff-Goldhaber, C. B. Dover, and A. L. Goodman, Annu. Rev. Nucl. Sci. **26**, 239 (1976).
[50] D. S. Delion, Phys. Rev. C **80**, 024310 (2009).